Process optimization-oriented deformation control of large aluminum alloy structures from high-speed EMU

Yana Li (lyn@djtu.edu.cn)
Dalian Jiaotong University https://orcid.org/0000-0003-1976-0758
Jiahao Liu
Dalian Jiaotong University
Zeyang Zhang
Dalian Jiaotong University
Changlun Dai
Dalian Jiaotong University
Xingfu Yin
Dalian Jiaotong University
Xinpeng Shi
Dalian Jiaotong University

Research Article

Keywords: large aluminum alloy structures, double ellipsoidal heat source, thermal elastic-plastic method, inherent strain method, process optimization

Posted Date: February 7th, 2024

DOI: https://doi.org/10.21203/rs.3.rs-3825599/v1

Abstract

Predicting and controlling the welding deformation of large aluminum alloy structures is crucial to ensure the accuracy during the manufacturing of high-speed electric multiple units (EMUs). On the basis of heat source calibration, the dual ellipsoid heat source model and simplified equation parameters were used for metal-inert gas (MIG) welding, and the simulation of residual stresses obtained from the three numerical simulation methods were compared with the experimental values, and it was determined that the thermoelastic-plasticity method was used as a method to establish a high-precision inherent strain database. Based on this database, the welding deformation of the entire sidewall (23 m, 44 welds) was predicted and compared with the experimental data, and the error of the two results was less than 1 mm, and the simulation model was able to reflect the actual situation. Meanwhile, on the basis of this model, the effects of welding sequence, spot fixing method and number of clamps on welding deformation were investigated separately, and the results showed that: the reasonable welding sequence reduced the maximum deformation by 30.90%; the appropriate spot fixing method reduced the maximum deformation by 12.56%; and the reduction of the number of clamps by 9% could get the same effect as the original scheme, and the reduction of the number of fixtures by 18% could still ensure that the overall deformation was basically unchanged. Thus, process optimization can effectively control welding deformation, providing insights for improving the welding quality of aluminum alloy-based high-speed EMUs structures.

1. Introduction

To meet the contemporary requirements of “weight reduction, speed up,” aluminum alloy materials have been widely used in rail vehicles, especially in high-speed EMUs. The bodies of different types of high-speed EMUs have been welded using different aluminum alloys with high coefficients of thermal expansion and shrinkage, which makes it challenging to weld and control the welding deformation [1, 2]. Determining and controlling welding deformation of large aluminum structures and improving welding quality via experimental process conditions are not economical and practically feasible; thus, welding numerical simulation calculations have wide application potential because of several advantages, such as low cost and high calculation accuracy [3].

For large structures, the thermal elastic-plastic method and the inherent strain method are the typically used numerical simulation methods. Using the thermal elastic-plastic method, the entire process of welding simulation can be tracked, the welding deformation of the structure can be obtained, and the temperature field and stress field results of each moment can be analyzed. However, the thermo-elasticity calculation process is a typical nonlinear process with large calculation time, and it does not easily converge. It is therefore suitable only for the numerical simulation of general welded joints and small structures of welding deformations [4–6]. Research on welding deformation prediction of large structures is still in nascent stages. Kazuki Ikushima et al. implemented the unitary method for predicting the deformation of vehicle side rails through a large-scale thermal elastic-plastic analysis method idealized to display finite elements, which can be modelled in a reasonable computational time. [7]. Paik J had

successfully predicted the residual stresses and deformations induced by welding of steel reinforced plate structures based on the three-dimensional thermal elasto-plastic finite element method taking into account the initial defects and experimentally verified its accuracy. [8]. Gao Xu obtained the influence mechanism of fixture positioning and welding sequence on the residual stress and deformation of side wall welding, considering the side wall of a high-speed train body as the research object; they analyzed the fixture positioning and welding sequence parameters based on the thermal elastic-plastic method [9].

The inherent strain method is a relatively economical means for predicting the deformation of large and complex welded structures, and it can obtain the residual stresses and deformation values with some accuracy. Thus, it has good practical significance and development prospects. Since the 1990s, Japanese researchers have introduced the theory of inherent strain in welding simulation studies, which have been widely applied in the marine industry [10–12]. Corresponding results have been achieved in butt welding, fillet welding, plane segment welding, and surface welding of large complex structures [13–15]. In the early 20th century, there was extensive new research on the inherent strain method for the welding deformation of rail vehicles. In 2004, Xie Lei et al. studied the inherent strain law of aluminum alloy butt welding and determined the relationship among longitudinal shrinkage, transverse shrinkage, and angular deformation with different heat input parameters. Then, they predicted the welding deformation of a simplified model of locomotive roof cover, providing a theoretical basis for controlling welding deformation [16]. There are several contemporary applications of the inherent strain method in the welding deformation prediction of rail vehicles, such as the electric locomotive pillow beam [17], bogie side beam [18], stainless steel roof [19], aluminum alloy floor [20], aluminum alloy end wall [21], and aluminum alloy body [9, 22]. These studies have provided theoretical insights for welding process optimization and welding deformation control for rail vehicles. Overall, the thermal elastic-plastic method is suitable for examining small and fine modeling structures or joints. It enables fine modeling and analysis of the temperature, deformation, and stress at each moment; however, it requires a lot of time-consuming calculations. The inherent strain method is suitable for studying the welding deformation of large structures. It disregards the temperature and stress changes at each moment, and only examines the final deformation. It requires less time-consuming and less extensive calculations. Therefore, it is more suitable for the prediction and control of welding deformation of large structures of railway vehicles.

The traditional thermal elastic-plastic theory cannot solve the simulation problem of large-size components. Most of the research on the thermal elastic-plastic method has focused on predicting the welding residual stress and deformation of small welded structures, and only used this method to verify test and simulation results and analyze process parameters without improving the heat source model that determines calculation accuracy. In recent years, scholars at home and abroad have applied the inherent strain method to the welding deformation prediction of various large structures, but the research objects have mostly been roofs, floors, and side beam structures. However, research on the large aluminum alloy side walls of high-speed EMUs, which are mainly composed of 5 large aluminum alloy profiles with different joint types, numbers of welds, and clamping constraints, is very limited. It is challenging to study the deformation of the whole structure. In addition, most current research has

focused on predicting welding residual stress and deformation in single-welded joint types of local side wall structures. It has only optimized welding process parameters from a single welding sequence, instead of test verification and multi-process parameter optimization. And the inherent strain method only considers the influence of longitudinal and transverse strains [23, 24], and the angular strain is not taken into account. There is also no research on controlling welding deformation of whole structures by optimizing process schemes.

This study focused on the aluminum alloy side-walls (length = 25 m) of a high-speed EMU. Combined with the actual production process parameters, a high-accuracy inherent strain database considering longitudinal, transverse, and angular strains of butt and lap welding joints was established using the thermal elastic-plastic method. The deformation influence of the welding sequence, tacking-weld setting, clamp number, and position were examined and compared with the experimental analyses. The findings of this study provide insights for welding deformation control of large aluminum alloy structures.

2. Local model simulation analysis and validation

2.1 Heat source calibration

The side-wall of a high-speed EMU welded from five pieces of 6005A aluminum alloy with extruded profiles was considered. Two types of welding joints were considered, namely, butt and lap joints. Heat source calibration was carried out on both to develop a heat source model for simulation calculations.

The actual side-walls were welded using MIG welding, thus the double ellipsoidal heat source model proposed by Goldak [25] was selected for simulation. The forming of the weld was controlled by the shape parameters of the double ellipsoidal heat source model. Changing these parameters enabled calculation of different heat source shapes, resulting in the formation of different welds and diverse temperatures of the melt pool, which affected the temperature field of the welded component and caused deviations in the calculated stress field, and deformation. The relevant parameters of the heat source model were constantly adjusted after the process parameters were determined, and the heat source shape consistent with the actual molten pool shape was obtained. In [26], the relationship between plate thickness and double ellipsoid heat source model was provided, and the shape parameters was calculated using Eq. (1) to check the heat source.

$$\begin{cases} a = 0.77h + 0.08 \\ b = 0.79h + 0.20 \\ a \le c_f \le h \\ 2c_f \le c_r \le 4c_f \end{cases} \quad (1)$$

where a, b, c_f, and c_r are the double ellipsoid shape parameters, and h is the plate thickness.

Table 1 Welding and heat source parameters of butt and lap joints

Welding parameter	Butt joint	Lap joint
Welding speed V	12 mm/s	13 mm/s
Welding current I	210 A	260 A
Welding voltage U	22 V	25 V
Heat source efficiency	75%	75%
Total energy input Qz	385 J/mm	480 J/mm
Net energy input	289 J/mm	360 J/mm

The welding process parameters are presented in Table 1; as shown in Eq. (1), double ellipsoidal heat source shape parameters were adjusted for the two types of welding joints. The calculated heat source cross section was compared with the joint heat source model obtained after physical experiment corrosion. The simulated heat source was close to the actual heat source result, as shown in Fig.1, which satisfied the molten pool boundary criterion. The measured molten pool area was also consistent with the actual heat source. Therefore, the established double ellipsoid heat source was suitable for using as a heat source model for MIG welding. The final determined parameters of the double ellipsoid heat source model are shown in Table 2.

Table 2 Heat source parameters

Heat source parameter	Butt joint	Overlap joint
Width a	3 mm	3.5 mm
Depth b	4 mm	5 mm
Front half-axle length c_f	3 mm	3.5 mm
Rear half-axle length c_r	12 mm	14 mm
Front half-axis energy distribution f_f	0.8	0.8
Rear half-axis energy distribution f_r	1.2	1.2

2.2 Local model introduction

To improve the accuracy of the simulation, the inherent strain database for the local model is typically calculated using three methods, namely, the thermal elastic-plastic method [27,28], thermal cyclic curve method [29,30], and shrinkage force method [31,32]. In this study, these three methods were used to simulate and analyze the local model using Simufact software; simulation and experimental results were compared to identify the best simulation calculation method, and then, the inherent strain database of the two types of welding joints was established.

A small part between the upper and middle window panels was selected as a local model (dimensions = 1000 mm × 600 mm). There were two butt joints in the local model (Figure 2(a)) which used the heat source model presented in Table 2. 3D Solid elements were used to simulate the local model, with 424,705 nodes and 370,800 elements.

Five measurement points A–E were selected on the workpiece transverse centerline; these were located on the weld, on the edge of the weld, on the heat-affected zone (near the weld), on the heat-affected zone (away from the weld), and on the base material, respectively, and were 3 mm, 8 mm, 23 mm, 36 mm, and 280 mm, respectively, away from the center line of the weld. These were also the measurement points of residual stresses as well as simulation model tracking points, as shown in Figure 2(b).

During the actual processing, combination clamping conditions of the supporting platform and square blocks were used, as shown in Figure 3 (a). The simulation analysis was therefore based on the actual processing, and the restraints considered the same clamping conditions, as shown in Figure 3 (b); the welding was done along the X-direction.

2.3 Validation analysis of residual stresses

Residual stresses in the butt joint structure, determined by simulation, were mainly attributed to longitudinal residual stress. To better compare the accuracy of the results obtained using the three

methods, the residual stresses calculated at five points (shown in Figure 2(b)) were selected. Comparison of simulated and measured values including longitudinal residual stress and relative error was shown in Figure 4. Furthermore, Table 3 provided a comprehensive explanation of each of the three methods. X-ray diffraction (XRD) was used for testing the residual stress of the joints. Because the test depth was only 20 μm, the additional stress layer on the surface was stripped by electrolytic polishing, and then, the actual distribution of the residual stress for welding was accurately measured. This mainly comprised five steps, namely, inspection, grinding, polishing, cleaning, and testing.

As shown in Fig. 4, the thermal elastic-plastic method had high calculation accuracy, and its curve was the closest to the measured curve, and the relative error was very small. The calculation results of the thermal cycle curve were also closer to the measured results, but the relative errors were large in the position away from the weld, while the calculation results of the shrinkage force method were the farthest from the measured curve, and the relative errors of each measuring point were large. This was because the thermal elastic-plastic method adopts a typical nonlinear process, which requires multiple iterations and is time consuming; however, it has high calculation accuracy. Furthermore, the thermal cycle curve method is based on the thermal elastic-plastic method, which further simplifies the moving heat source of the thermal elastic-plastic method. The shrinkage force method is based on the calculation theory of empirical accumulation and has poor accuracy. Therefore, this method will not be considered in the following discussion.

The simulated results of points A and B near the weld were far from each other from a single curve. This was because welding heat was most concentrated at the center of the weld, and the working conditions were complex and varied. Therefore, the absolute error of the numerical value on the center of the weld obtained by simulation calculation was larger than that in other regions, but it did not exceed 10% and the relative error was small. Except for shrinkage force method, the simulated results of points C–D were close to measured results and had low relative error based on the thermal elastic-plastic method and the thermal cycle curve method. The absolute error was only approximately 5%. The simulated results of point E was close to measured results although high relative error, this was because point E was far away from the weld, the temperature gradient was small, resulting in a small residual stress value, so a small absolute error would induce a large relative error at point E.

As shown in Table 3, under the same computer configuration, the same model, and the same mesh size and number, the calculation time of the three methods varied considerably, and the calculation error was also large. The thermal elastic-plastic method had high calculation accuracy and long calculation time, which made it suitable for small models that require high calculation accuracy. The thermal cycling curve method had relatively high calculation accuracy, and its calculation time was significantly smaller than that of the thermal elastic-plastic method, making it suitable for models of medium and large structures with high calculation accuracies. The shrinkage force method had lower calculation accuracy, making it suitable for models of large structures with low calculation accuracies. Thus, the thermal elastic-plastic method was used to simulate local models for obtaining high precision results of inherent strain values.

Table 3 Comparison of three methods

Methods	Thermal elastic-plastic method	Thermal cycling curve method	Shrinkage force method
Computer configuration	CPU: Intel(R) i9-11900K @ 3.50 GHz; Memory: 3000 MHz 64 GB		
Model size.	1000 mm × 600 mm × 50 mm		
Model scale	Nodes: 424,705 Elements: 370,800		
Calculation time	72 h 10 min	43 h 20 min	25 min
Residual stresses error	Minimal	Smaller	Larger
Range of application	Small structure	Medium and large structure	Large structure

2.4 Inherent strain database establishment

In several studies, longitudinal and transverse shrinkage are only considered when using the inherent strain method, and angular deformation is not taken into account. The influence of transverse, longitudinal, and angular deformation should be considered for such large structures of EMU side walls, with >20 m of welds with butt and lap welding joints [33]. Structural welding deformation simulations therefore require a database of inherent strains in all welding joints.

Main steps for establishing the inherent strain database.

(1) Two welding joints were extracted from the overall model, and a 3D solid mesh was created, as shown in Figure 2(a).

(2) Based on the thermal elastic-plastic method, the two welding joints were simulated considering the temperature, material, and non-linearity of heat transfer.

(3) There were significant temperature changes between the arc starting and arc stopping stages of the weld, so the intermediate weld area was selected to extract the relevant data, and it was summarized to obtain the inherent strain database.

The inherent strain databases of the two welding joints are presented in Table 4.

3. Overall model simulation analysis and validation

3.1 Overall model introduction

Overall side-wall comprised five parts, namely, upper wall panel, upper window panel, middle window panel, lower window panel, and lower wall panel (Figure 5(a)).The height and length were 1,873 mm and 23,756 mm respectively. The side-wall model had eight welds, which included seven butt joint welds and one lap joint weld (Figure 5(b)). Weld1, Weld4, Weld5, and Weld8 were continuous long welds; Weld2, Weld3, Weld6, and Weld7 were short welds because of the presence of the intermediate window. Therefore, there were total of 44 welds in the model, with 40 short welds and 4 long welds.

The overall model of the side-wall was a mesh of all shell elements. In terms of the calculation efficiency, the mesh at the weld seam was densely divided, with element size of approximately 2.5 mm, while the parent material mesh was sparsely divided, with element size of approximately 12 mm; the number of nodes and meshes was 374,545 and 433,132, respectively.

3.2 Welding simulation

The welding software Virfac was used to simulate the whole model, considering the computational efficiency and economy of the whole model. The overall welding simulation process was as follows: fixing with clamps; tacking welds of the whole workpiece; welding: Weld6, Weld7, Weld5, Weld8, Weld2, Weld3, Weld1, and Weld4; checking welding simulation deformation; and comparing with the actual measured deformation.

The inherent strain method was adopted to simulate welding deformation of the overall structure according to the actual welding process; results are presented in Figure 6.

As shown in Figure 6, the largest value of deformation was at the upper door frame of the left side door (6.305 mm); the second largest deformation was at the lower right side of the inner door frame (5.171 mm); the third largest deformation was at the left side of window 1 (3.684 mm). The deformation around windows 4, 5, 8, and 9 was approximately 3.400 mm; it was approximately 1.800 mm in Weld4 and Weld8 (lap joints) and 1.600 mm in Weld1 and Weld5. In the remaining blue positions, the deformation was relatively small (not exceeding 1.000 mm). In short, the location and quantity of the clamps controlled the deformation of the whole side wall. The deformation of the upper door frame of a side door was the largest. This was because there was no clamp in this place, which was in a free state, resulting in the largest deformation. Other places with large deformation were mainly far away from the location of the clamp, or in the middle of the whole side wall, resulting in large deformation. The rest of the deformation was not large because of the setting of the clamp.

3.3 Validation

After side-wall welding according to the actual process, a type of calipers (manufactured to match the curvature of the outer surface of the side-wall) was used to measure the actual welding deformation. The

gap distance between the caliper blade and the side-wall was the amount of welding deformation, as shown in Figure 7.

To better compare the simulated deformation results with the actual welding results, three measurement locations were selected in the front, middle, and rear of side-wall (red line locations), as shown in Figure 8 (a). At the same time, two welding deformation measurement points were selected on the outside of each aluminum profile along the section direction, as shown in Figure 8 (b); thus, there were a total of 30 measurement points. And each measuring point was measured several times and averaged. The gap distance of 30 measurement points were used to evaluate the deformation of the side-wall.

Comparison of deformations between simulation and experiment was shown in Figure 9. As shown in Figure 9, at all three locations, the overall deformation showed a similar trend. The deformation value of measured location 3 was larger than that of measure location 1, because the weld length was long and clamping number was less in this position. The deformation value of location 2 was between position 1 and location 3. At the same location, the deformation value of 1-5 measured points were less than that of 6-10 measured points, because the latter was located on the large structural curvature to increase the risk of welding deformation. From the whole 30 deformation measurement points, at 9 measurement points, error was <0.1 mm, at 16 measurement points, it was >0.1 mm and <0.5 mm, and at 5 measurement points, it was >0.5 mm and <1 mm. Thus, it is reasonable, consistent, and correct to calculate the welding deformation of the side-wall of high-speed EMUs using the inherent strain method.

4. Influence of welding process conditions on deformation

4.1 Welding sequence influence

Different welding sequences affect the amount of welding distortion as well as the number of overturn flips on the entire side-wall. Welding simulation can be performed without considering field operations; however, in the actual welding process, the number of overturn flips should be considered. The length of the side-wall of the high-speed EMU was approximately 23 m; three schemes were therefore selected, as shown in Table 5. Scheme three is ideal for simulation, and it can be used to compare other welding sequences for examining the influence of welding deformation.

The total deformations for the three schemes were calculated and compared with the original scheme, as shown in Figure 10.

Compared with the original scheme, in scheme one, the outer side wall was welded first and then the inner side was welded. In the original scheme, welding was done from the middle to both sides. In scheme one, welding was done from top to bottom, and the clamp was turned over once, ensuring that the overall welding deformation did not change much. In scheme two, alternate welding from the outer to inner sides was carried out, and the clamp was turned over four times; as a result, its welding deformation was considerably different compared with other schemes. In scheme three, inner and outer side alternate welding was carried out, and the clamp was turned over seven times. In scheme three, the maximum

deformation decreased from 7.072 mm to 4.887 mm, and the second largest deformation decreased from 6.467 mm to 3.59 mm. Scheme three was thus the best scheme; however, scheme one was optimal considering the overturn flips. Thus, the welding sequence considerably influenced the welding deformation.

4.2 Tack-weld influence

In actual production, two types of tack-weld settings are often used on structures. One was used to set the tack-weld for assembling a whole structure before welding (named scheme one, as shown in Figure 11), and the other was used to set tack-weld only when the specific part was welded (named scheme two).

Two types of tack-weld setting simulations were studied, as shown in Figure 12. As shown in Figure 12, the maximum welding deformation obtained by scheme two was significantly less than that using scheme one. The maximum decrease in deformation at other positions was less for scheme one than for scheme two. This was because in scheme one, five aluminum profiles were combined into a whole by setting tack-weld; as a result, the internal stress of the eight welds was added to the whole workpiece. The maximum deformation and the second largest deformation were influenced by the eight welds, resulting in larger deformation. In scheme two, five aluminum profiles were welded separately; the internal stress produced during welding did not affect other parts, so the maximum deformation and the second largest deformation were small and only affected by a few neighboring welds.

4.3 Influence of number of clamps

In practical production, external clamping constraints are typically used to control welding distortion. Welding deformation decreases with increase in the number of clamping constraints; however, this increases the production cost. This simulation analysis showed that welding deformation of the model was within a reasonable value range. Combining these findings with the actual deformation, fewer number of clamps can be used at locations with smaller deformations to reduce production costs.

The deformation between windows 2 and 3 and 6 and 7 was small; therefore, we attempted to reduce the number of clamps at these two positions. Three clamping schemes were set as shown in Table 6.

Simulation calculations show that these three clamping scheme conditions only slightly influenced the maximum deformation, but they considerably influenced the local deformation. To better analyze the influence of reduced number of clamps on local deformation, the deformation between windows 2 and 3 and 6 and 7 were compared for the different clamping schemes, as shown in Figure 13.

As shown in Figure 13, compared with the original scheme, clamping scheme one decreased the number of clamps at the upper and lower wall panels, and the deformation was not considerably different. Both clamping schemes two and three had local deformations of approximately 2.20 mm, and the

deformation area of clamping scheme three was larger than that of clamping scheme two. The clamping of the upper and lower wall panels between windows 2 and 3 and 6 and 7 had a more obvious deformation effect than the clamping configuration on the other panels.

5. Conclusion

Addressing the complexity, joint diversity, large number of welds, and long weld lengths found in the aluminum alloy sidewall structure of large high-speed EMU, an in-depth study has been conducted on welding deformation prediction and control. Through experimental verification, the accuracy of finite element model simulation has been confirmed, providing a solid theoretical foundation and practical guidance for optimizing the welding process scheme and accurately controlling welding deformation in rail vehicles.

(1)A heat source model for MIG welding of two aluminum alloy joints has been successfully simulated to account for their unique characteristics. The study demonstrates that the simplification of the heat source shape parameter formula, utilizing the double ellipsoidal heat source model, enables rapid and accurate simulation of the heat source effect. This approach reduces the redundant process of heat source calibration and significantly decreases simulation time. Following heat source calibration, the weld molten metal region in the model aligns closely with experimental results, thereby validating the reliability of the simplified heat source shape parameter formula and the accuracy of the heat source model.

(2)To identify a suitable method for the research object in this paper among various existing simulation methods, a comparison of three methods is conducted: the thermal elastic-plastic method, the thermal cycle curve method, and the shrinkage force method. The results indicate that the thermal elastic-plastic method offers a significant advantage in terms of calculation accuracy, with its simulation curves aligning most closely with the measured curves. Conversely, the thermal cycle curve method simplifies the heat source movement process, leading to a slightly lower computational accuracy compared to the thermal elastic-plastic method. The shrinkage force method, on the other hand, relies primarily on accumulated experience and exhibits relatively low accuracy. Consequently, for the local model, it is decided to employ the thermal elastic-plastic method to establish a high-precision inherent strain database that ensures the accuracy of subsequent simulations.

(3)Exciting conclusions have been drawn regarding the prediction of weld distortion in large aluminum alloy sidewall structures. The simulation calculation is highly consistent with the actual measurement trend, with 83.33% of the total measurement points having an error of less than 0.5 mm and 100% of the measurement points having an error of less than 1 mm. This indicates that the established simulation model can truly reflect the actual situation.

(4)In addition, the effects of reasonable welding sequence, appropriate tack-weld settings, and reducing the number of clamps on the maximum distortion are also investigated. The results indicate that a reasonable welding sequence can significantly reduce the maximum distortion by 30.90%, and an

appropriate tack-weld setting can reduce the maximum distortion by 12.56%. Surprisingly, reducing the number of clamps by 9% can achieve the same effect as the original scheme, while reducing fixtures by 18% can still keep the overall deformation basically unchanged, except for the slightly larger value of individual point positions. This provides a solid foundation for optimizing the actual production welding process. By optimizing the welding process, production conditions can be reduced, thereby improving production capacity and factory productivity.

Declarations

Acknowledgements

This work was supported by the financial support from National Natural Science Foundation of China (Grant No. 52075066) and Liaoning Provincial Department of Education Project from China(Grant No. LJKZ0497).

The authors would like to thank all the reviewers who participated in the review, as well as MJEditor (www.mjeditor.com) for providing English editing services during the preparation of this manuscript.

Data availability statement

The data used to support the findings of this study are available from the corresponding author upon request.

Conflicts of interest

The authors declare no conflict of interest.

References

1. Verma RP, Lila MK (2021) A short review on aluminium alloys and welding in structural applications. Materials Today: Proceedings 46: 10687–10691. https://doi.org/10.1016/j.matpr.2021.01.447
2. Leon JS, Bharathiraja G, Jayakumar V (2020) A review on friction stir welding in aluminium alloys. IOP conference series: materials science and engineering 954: 012007. https://doi.org/10.1088/1757-899X/954/1/012007
3. Tambunan S, Yatim A, Sanjaya PW et al (2019) In-Service Welding Simulation of 28 Pipeline Using Finite Element Method. IOP Conference Series: Materials Science and Engineering 694: 012028. https://doi.org/10.1088/1757-899x/694/1/012028
4. Ahmad SN, Manurung YH, Prajadhiana KP et al (2022) Numerical modelling and experimental analysis on angular strain induced by bead-on-plate SS316L GMAW using inherent strain and

thermomechanical methods. Int J Adv Manuf Technol 120:627–644. https://doi.org/10.1007/S00170-022-08684-5

5. Asadi P, Alimohammadi S, Kohantorabi O et al (2021) Numerical investigation on the effect of welding speed and heat input on the residual stress of multi-pass TIG welded stainless steel pipe. Proceedings of the Institution of Mechanical Engineers, Part B: Journal of Engineering Manufacture 235: 1007–1021. https://doi.org/10.1177/0954405420981335
6. Marques ES, Silva FJ, Pereira AB (2020) Comparison of finite element methods in fusion welding processes—a review. Metals 10:75. https://doi.org/10.3390/met10010075
7. IKUSHIMA K, MAEDA S, UCHIMURA T et al (2020) Prediction of Welding Deformation of Automotive Components Using Large-scale Thermal Elastic Plastic Analysis. QUARTERLY JOURNAL OF THE JAPAN WELDING SOCIETY 38: 149s-153s. https://doi.org/10.2207/QJJWS.38.149S
8. Paik J (2018) Three-dimensional thermo-elastic-plastic finite element method modeling for predicting weld-induced residual stresses and distortions in steel stiffened-plate structures. World J Eng Technol 6:176–200. https://doi.org/10.4236/wjet.2018.61010
9. Gao X (2018) Research on Welding deformation mechanism of complex aluminum alloy thin plate structures. Shandong University, CHINA
10. Mochizuki M, Mikami Y, Yamasaki H et al (2007) Elastic predicting method of weld distortion of large structures using numerical simulation results by thermal-elastic-plastic analysis of small components. Weld World 51:60–64. https://doi.org/10.1007/BF03266609
11. Mondal AK, Lohit A, Biswas P et al (2018) Prediction of weld-induced distortion of large structure using equivalent load technique. Proceedings of the Institution of Mechanical Engineers, Part B: Journal of Engineering Manufacture 232: 499–512. https://doi.org/10.1177/0954405416646309
12. Murakawa H (2007) Computational welding mechanics and concept of inherent strain for industrial applications. Mater Sci Forum 539:181–186. https://doi.org/10.4028/www.scientific.net/MSF.539-543.181
13. Ndiwe B, Kah P, Njock Bayock FM et al (2023) Numerical and experimental investigations of mechanical properties of AW 6005-T6 Aluminium alloy butt weld joint using GMAW process. Metall Mater Eng 29:16–36. https://doi.org/10.56801/MME907
14. Bajpai T, Nyati AK, Sharma P et al (2023) Numerical and Experimental Investigation on Effects of Welding Sequence on Distortions in Fillet-Welded AA6061-T6 Joints. J Mater Eng Perform 1–15. https://doi.org/10.1007/s11665-023-08755-y
15. Murakawa H, Deng D, Ma N et al (2012) Applications of inherent strain and interface element to simulation of welding deformation in thin plate structures. Comput Mater Sci 51:43–52. https://doi.org/10.1016/j.commatsci.2011.06.040
16. Xie L, Luo Y, Xie Z et al (2004) Prediction of deformation of large welding fabrication based on inherent strain. Trans CHINA Weld INSTITUTION 25:107–114
17. Wang Y, Luo Y, Liu H (2015) Prediction of welding deformation on electric locomotive body bolster by considering welding sequence. Trans CHINA Weld INSTITUTION 36:101–110

18. Afazov S, Mistry K, Uzunov K (2023) Welding simulation of railway bogie frame side beam: Analyses of residual stresses, clamping forces, distortion and prediction of fatigue S-N curves. Proceedings of the Institution of Mechanical Engineers, Part F: Journal of Rail and Rapid Transit 237: 33–40. https://doi.org/10.1177/09544097221094986
19. Li S, Zhu H, Dai Z (2018) Simulation of welding deformation of stainless steel car body roof based on inherent strain method. Electr Weld Mach 48:9–12
20. Wei S (2019) Research on friction stir welding of metro floor based on numerical simulation. https://doi.org/10.26990/d.cnki.gsltc.2019.000352. Dalian Jiaotong University, CHINA
21. Zhao Y, Ding J, Liang L et al (2019) Finite element analysis of welding deformation and residual stress in large structure of railway vehicles. Weld Join 11:13–19
22. Li Y (2020) Simulation study on residual stress and deformation of large welded structure of hollow aluminum alloy with MIG. https://doi.org/10.26990/d.cnki.gsltc.2020.000243. Dalian Jiaotong University, CHINA
23. Chi Z, Liu Y, Wang L et al (2017) Simulation of FSW deformation of subway sidewall based on inherent strain method. Electr Weld Mach 47:1–7
24. Song K, Zhan X, Xu L et al (2021) Numerical simulation on laser hybrid welding deformation of side walls of train body based on inherent strain method. Weld Join 12:42–47
25. Yi M, Park J (2022) Study of heat source model and residual stress caused by welding in GMAW of Al alloy. Metals 12:891. https://doi.org/10.3390/MET12060891
26. Li Y, Liu J (2021) Simplified model of heat source shape parameters of double ellipsoid based on welding quality. Weld Join 8:7–1162
27. Zhu Z (2013) Analysis of residual stress and deformation for side beam on bogie. Southwest Jiaotong University, CHINA
28. Lu Y, Lu C, Zhang D et al (2019) Numerical computation methods of welding deformation and their application in bogie frame for high-speed trains. J Manuf Process 38:204–213. https://doi.org/10.1016/j.jmapro.2019.01.013
29. Huang X, Li N (2019) Simulation Analysis and Prediction of Welding Deformation of Large Steel Structure Frame Based on Simufact. Hot Working Technol 48:147–152. https://doi.org/10.14158/j.cnki.1001-3814.2019.21.037
30. Sun J, Dilger K (2023) Reliability analysis of thermal cycle method on the prediction of residual stresses in arc-welded ultra-high strength steels. Int J Therm Sci 185:108085. https://doi.org/10.1016/J.IJTHERMALSCI.2022.108085
31. Wang Y (2015) Investigation and application on the analysis methods of welding distortion in large-scale and complex marine structures. ShanghaiJiaoTongUniversity, CHINA, Shang Hai
32. Liu J, Li Z, Liu T et al (2021) A novel compliant assembly variation analysis with consideration of initial deviation and welding shrinkage. Ocean Eng 237:109636. https://doi.org/10.1016/J.OCEANENG.2021.109636

33. Vishvesha A, Pandey C, Mahapatra MM et al (2017) On the estimation and control of welding distortion of guide blade carrier for a 660 MW turbine by using inherent strain method. Int J Steel Struct 17:53–63. https://doi.org/10.1007/s13296-016-0098-4

Tables

Tables 4 to 6 are available in the Supplementary Files section.

Figures

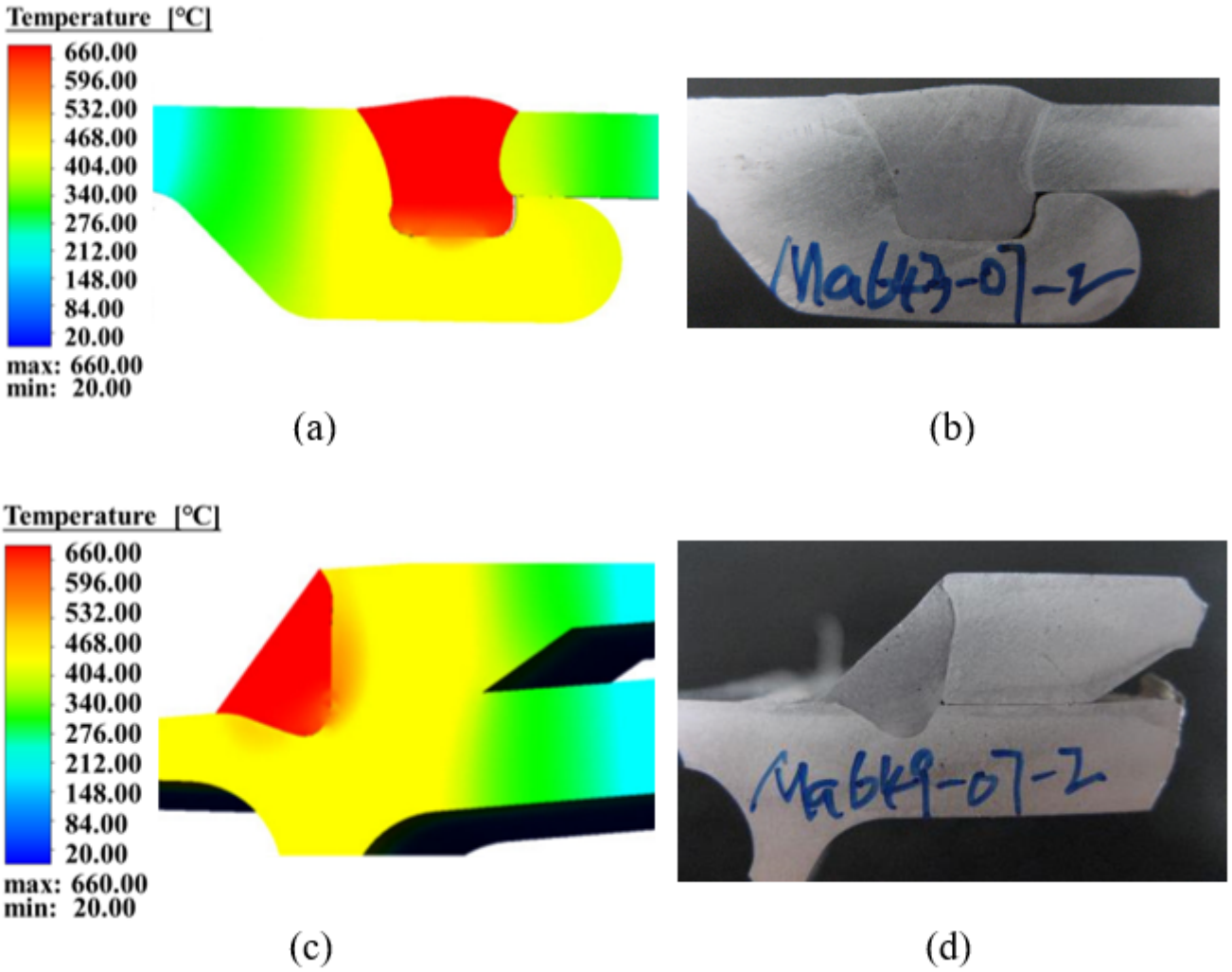

Figure 1

Heat source comparison: butt joint (a) simulation and (b) experimental results; overlap joint (c) simulation and (d) experimental results

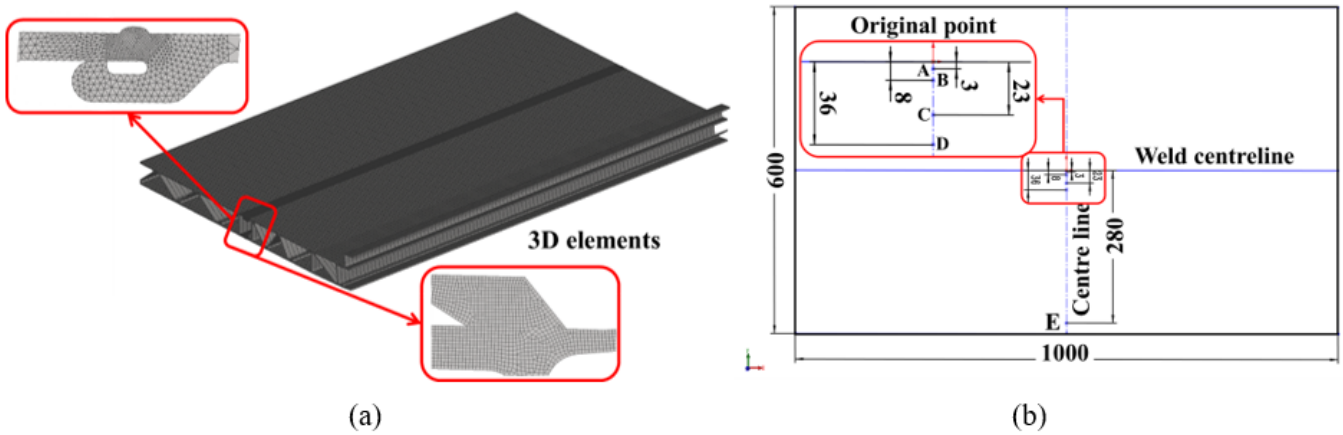

Figure 2

(a) Local FEM model and (b) location of measurement points

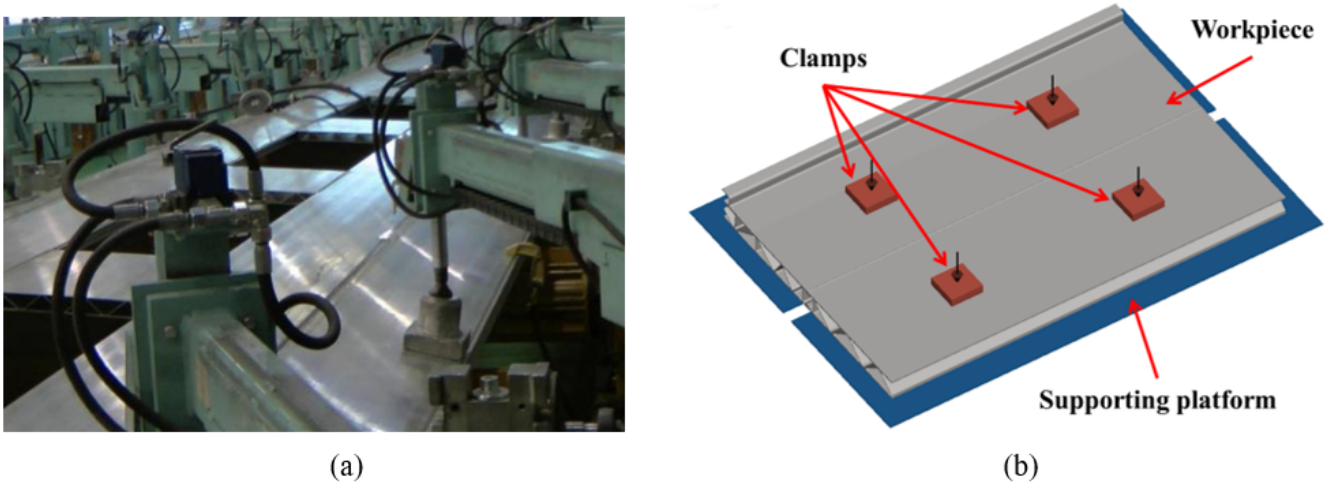

Figure 3

Clamping constraint model: (a) actual and (b) calculated clamping constraints

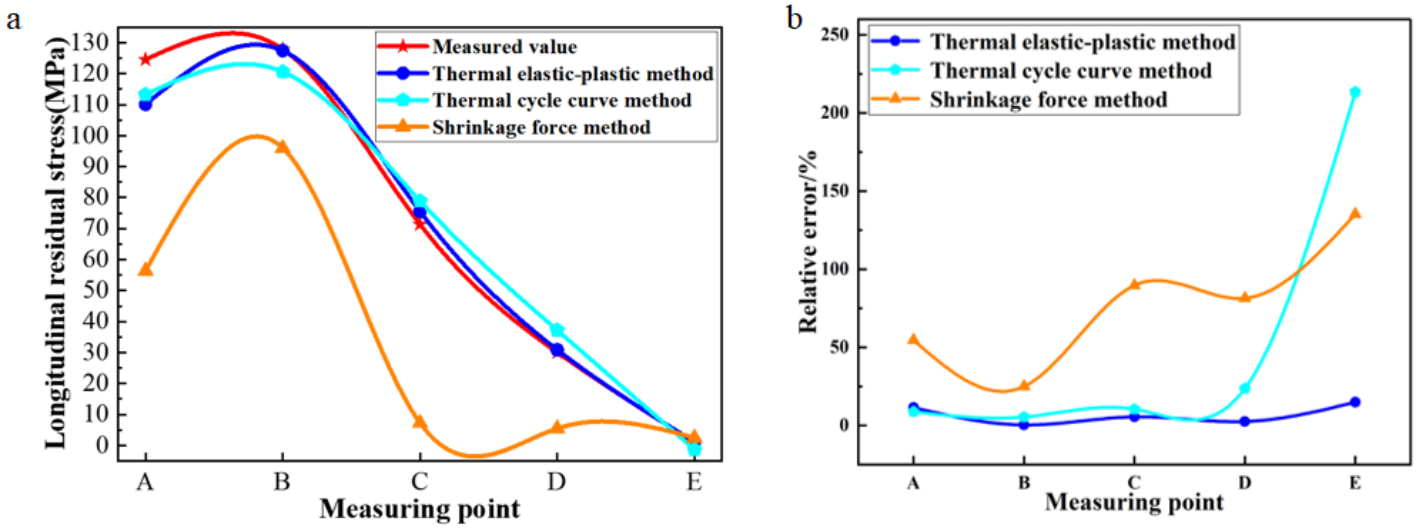

Figure 4

Comparison of simulated and measured values(a) longitudinal residual stress(b) relative error

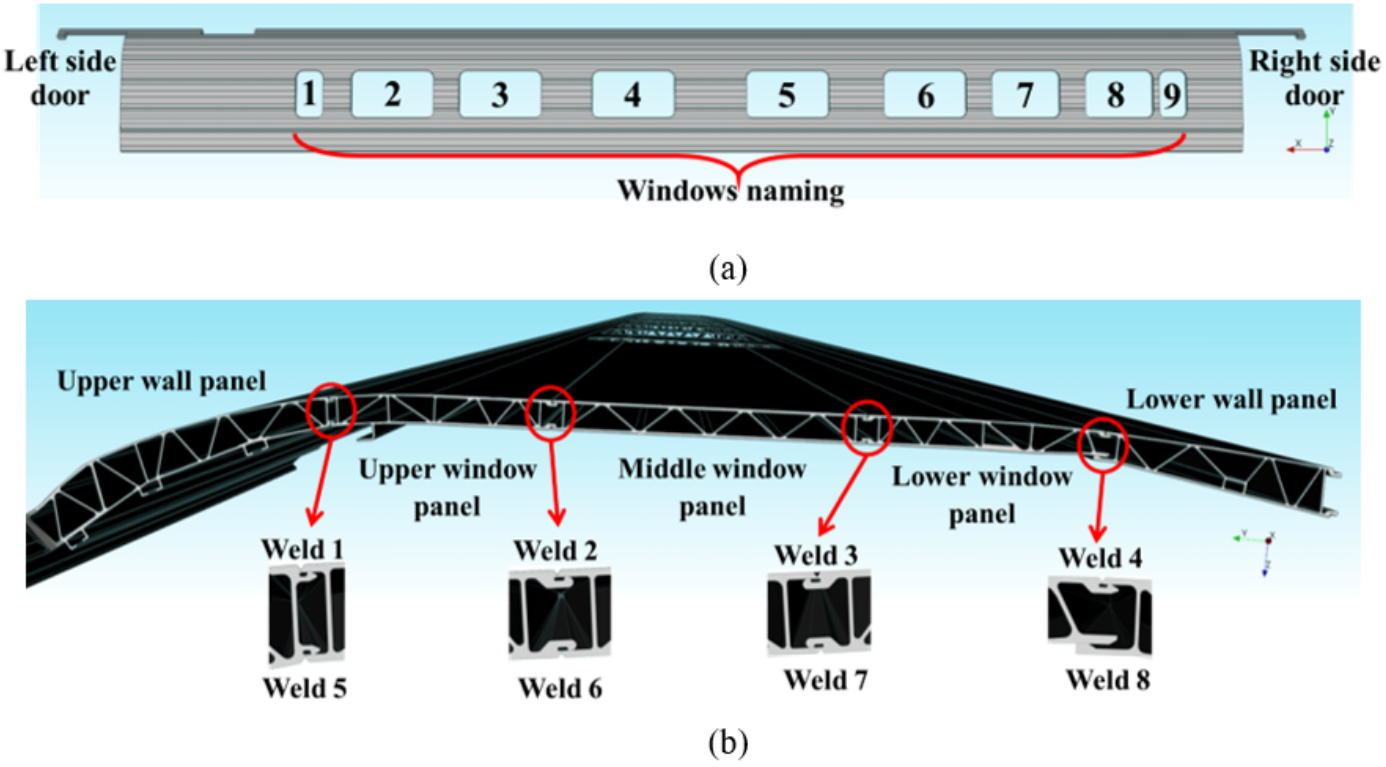

Figure 5

Side-wall model and joint types: (a) side-wall model; (b) joint types

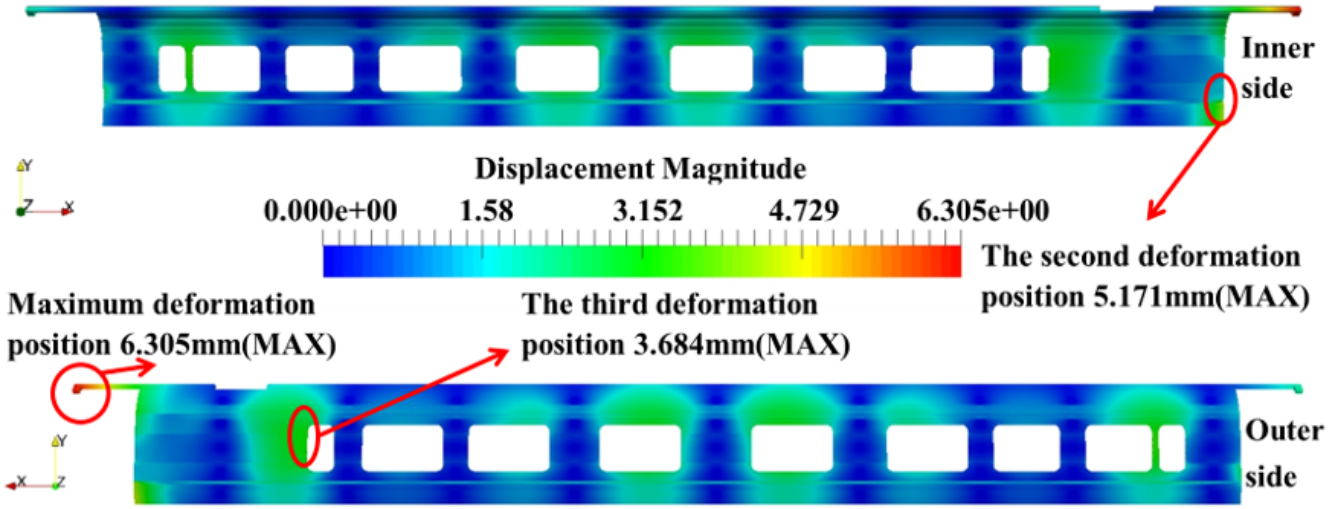

Figure 6

Simulated deformation

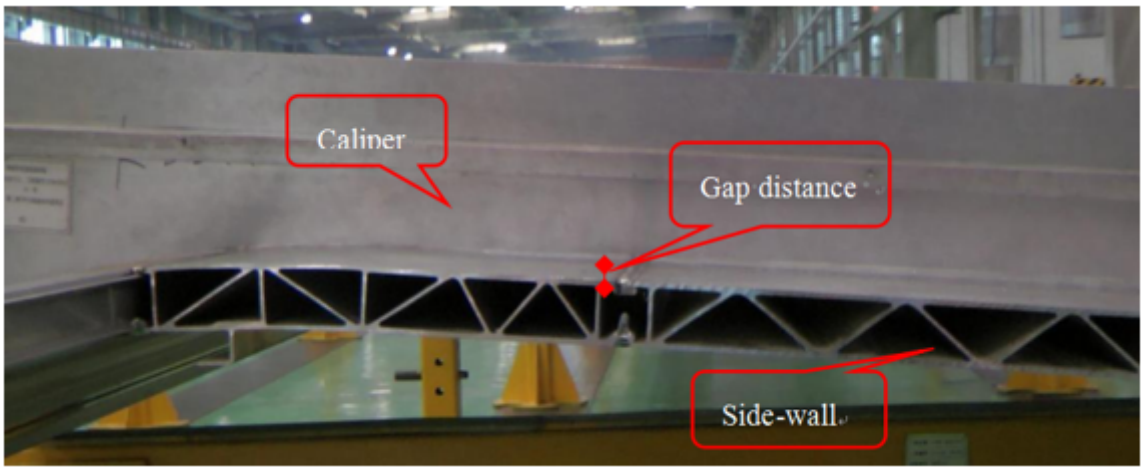

Figure 7

Measured deformation

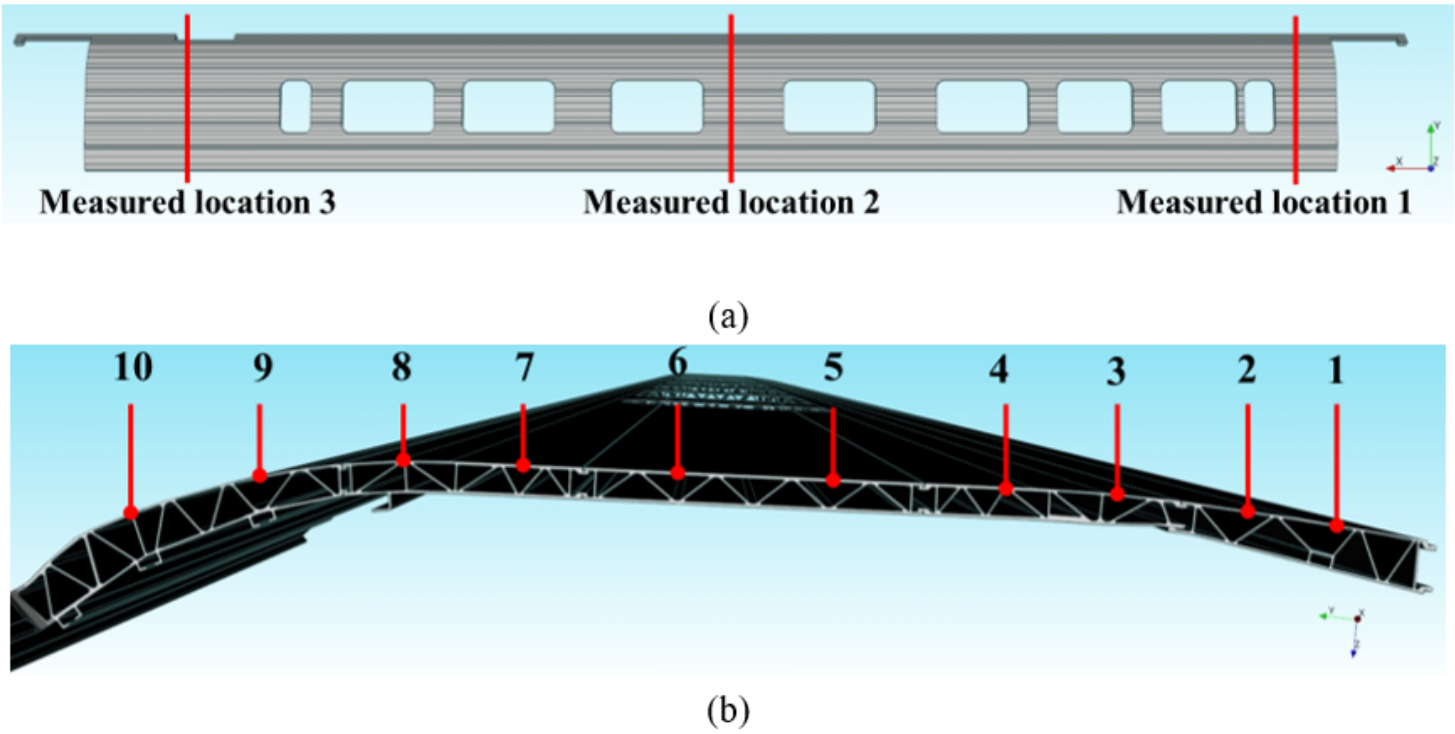

Figure 8

Deformation measurement sketch map: (a) measured locations; (b) measured points

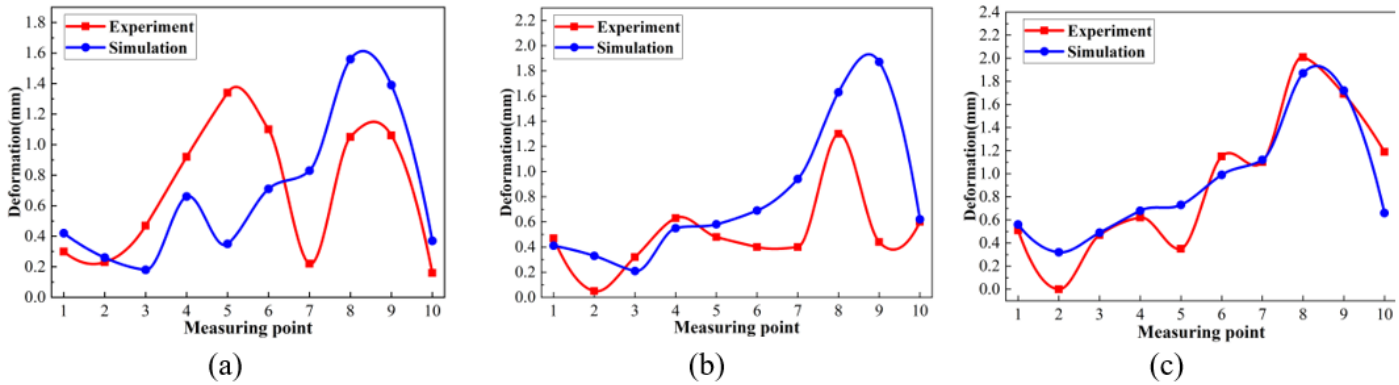

Figure 9

Comparison between simulated and measured deformations: (a)–(c) measured locations 1–3, respectively

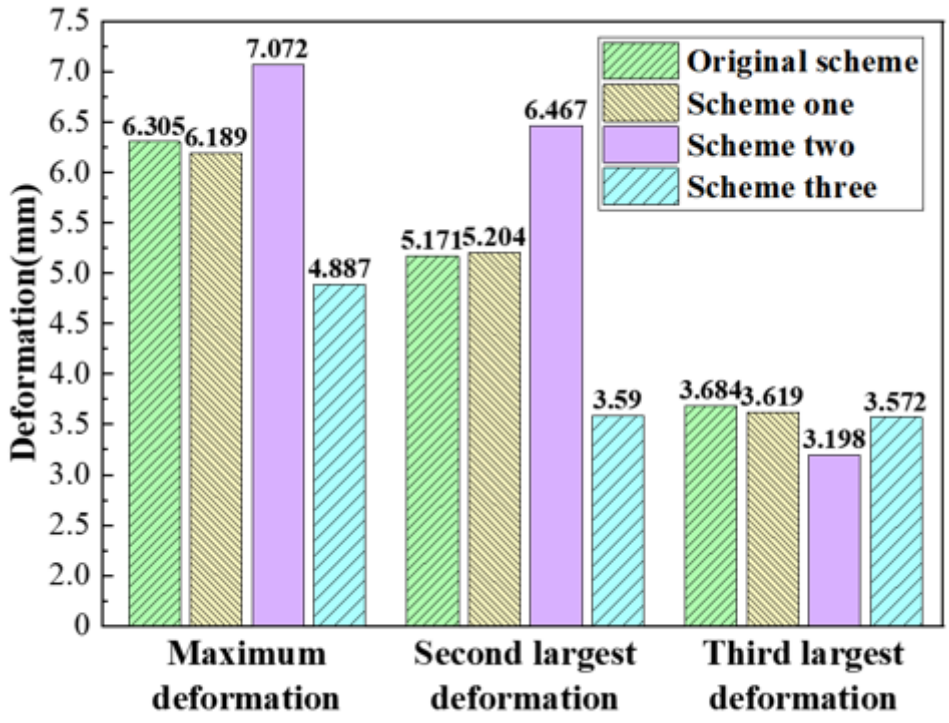

Figure 10

Comparison of the maximum deformation at the three main deformation positions

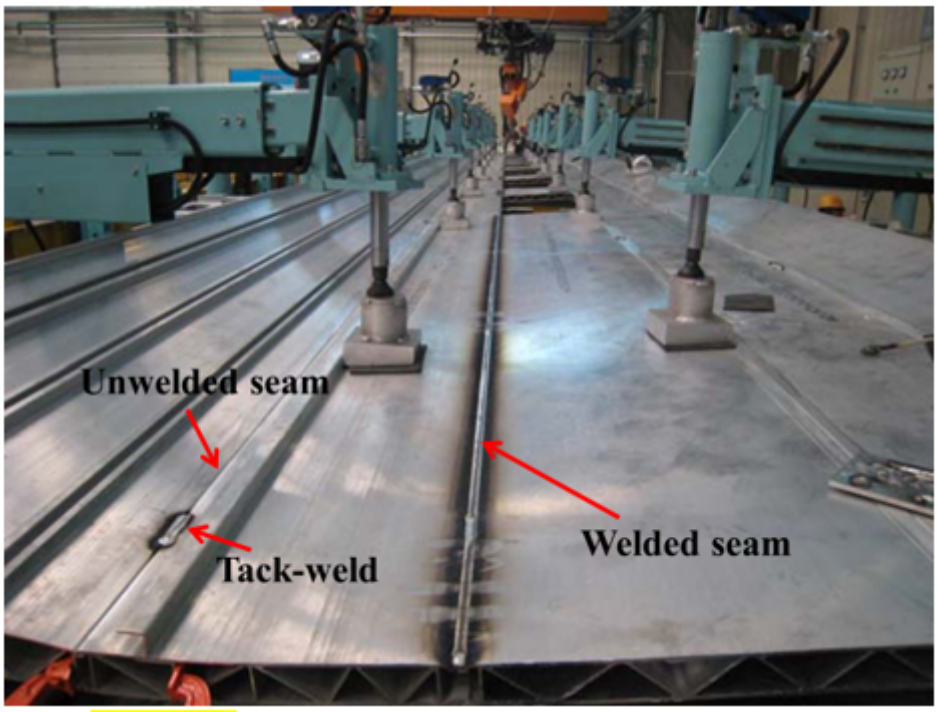

Figure 11

Tack-welds in actual production

Figure 12

Comparison between two schemes

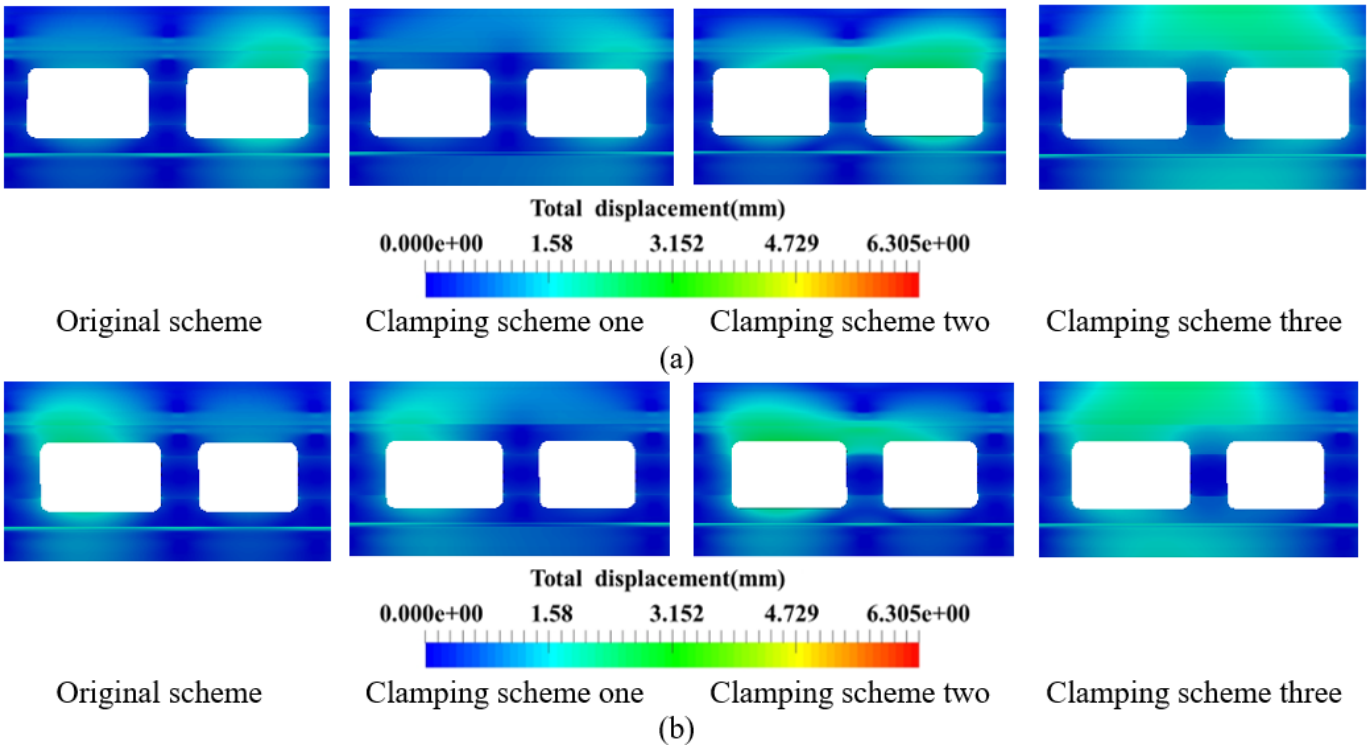

Figure 13

Comparison of local deformations from different clamping schemes: (a) Local deformation between windows 2 and 3 and (b) windows 6 and 7

Supplementary Files

This is a list of supplementary files associated with this preprint. Click to download.

- Table4Mainparametersoftheinherentstraindatabase.docx
- Table5Weldingsequencescheme.docx
- Table6Clampingscheme.docx